Colloid and Interface Science Communications 19 (2017) 20–24

Contents lists available at ScienceDirect

Colloid and Interface Science Communications

journal homepage: www.elsevier.com/locate/colcom

Rapid Communication

Modelling and Simulation of Drag Forces of Non-spherical Particles Moving Towards a Surface in Polymer Melt Flows

Eliana Agaliotis*, Celina Bernal

Universidad de Buenos Aires, Facultad de Ingeniería, Ciudad Autónoma de Buenos Aires, Argentina
CONICET - Universidad de Buenos Aires, Instituto de Tecnología en Polímeros y Nanotecnología (ITPN), Av. Las Heras 2214, C1127AAR, Ciudad Autónoma de Buenos Aires, Argentina

ARTICLE INFO

Keywords:
Computer simulation
Hydrodynamic drag force
Boundary interface effects
Laminar flow

ABSTRACT

This work deals with the drag forces acting on non-spherical particles translating normal to a surface in a polymer melt in which the particle–surface distance is small compared with particle dimension in the flow direction. Hence, drag forces will be modified as a function of distance. A finite element model was used in order to calculate the drag forces for the motion of particles. Several non-spherical particles geometries were simulated towards a plane surface wall.

The fitting of the numerical results with empirical expressions presented two very well defined tendencies. Up to a given value of particle-wall distance the influence of the wall was strong, hence it was necessary to apply a correction to the analytical calculations. In addition, the relevance of the shape of the channel between the particle and the sink was demonstrated. The computational results provided a clear benefit to validate empirical approaches using analytical approximations.

1. Introduction

The study of particle motion and the hydrodynamic interactions between individual particles is a logical first step oncoming to understand the hydrodynamic behavior of suspensions and especially determining process design calculations in several industrial processing applications. The hydrodynamics control the distribution of particles hence determine the dynamical behavior of the particles. The drag force effect is of particular applicability in the study of colloidal dispersions and colloid–polymer mixtures [1]. As an example, in sedimentation the major problem comes from the lack of spatial location control of the particles within the bed of particles or near fixed walls. Sedimentation velocity depends on the drag coefficient (i.e. the drag force) which is modified by the proximity of the particles to the wall. Hence, affecting sedimentation velocity. Other typical examples include filtration or phase-change material processing when part of the viscous liquid material fluid flows around a particle.

Most of the studies of drag forces in the Stokes regime ($Re < 1$) mainly address empirical correlations for spheres and usually are formulated for free falling velocity. For example, Zhong et al. presented the state of art in numerical modelling and theoretical development for particle-fluid flows, particularly focusing on non-spherical particles [2]. In that review, models and techniques describing the forces between particles and fluid in the case of spherical and non-spherical particles were highlighted, but in none of these studies the movement of the particle towards a wall was taken into account. In addition, there are other similar articles where the drag coefficients for non-spherical particles were determined, but in all of the studies the drag coefficients were calculated for free fall conditions [5–8].

In the present work, on the other hand, the drag force on a particle immersed into a polymeric matrix flowing near a wall or surface taken as a sink was investigated. Experimental results focusing on this topic were previously reported by Ambari et al., but only for spherical particles [9]. These results were compared here with our results obtained from simulation. However, our model not only simulates spherical particles but also addresses non-spherical particles.

The dynamics of non-spherical particles is considerably more complex than that of spherical particles, particularly, the particle-fluid interaction force. The movement of the particle is not parallel to the wall, hence, the drag force changes as a function of the surface distance in the flow direction [10–11].

The drag force was calculated here considering the influence of particle shape, the distance h to the surface and the fluid rheological properties.

* Corresponding author.
E-mail address: eagaliotis@fi.uba.ar (E. Agaliotis).

http://dx.doi.org/10.1016/j.colcom.2017.06.004
Received 14 March 2017; Received in revised form 2 June 2017; Accepted 21 June 2017

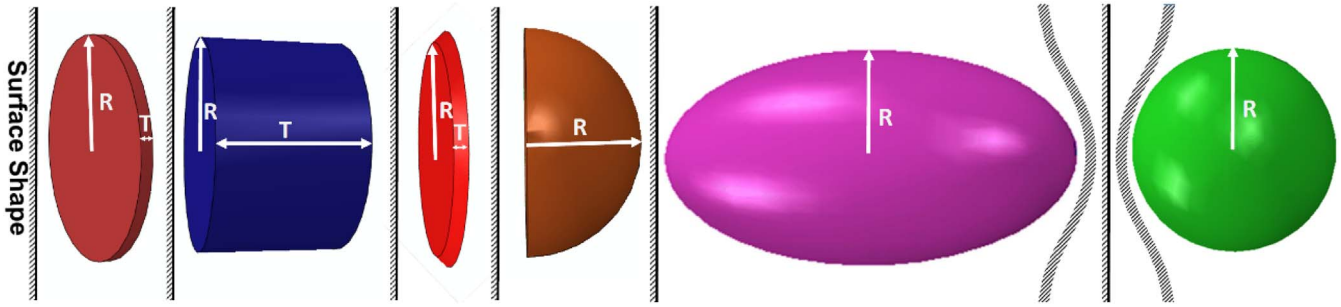

Fig. 1. Isometric perspective views of the particles used in the model. In all cases, the interface approaches the particle from the left in the direction of its axis of symmetry.

2. Methods: Model Description

A Computational Fluid Dynamics (CFD) model was implemented to calculate the drag force onto a particle immersed into a polymeric matrix near a wall taken as a sink. The results were compared with those obtained in the literature from analytical expressions and also with experimental results for the case of spherical particles [9,12–13].

The physical system used in the calculations was a solid particle with different shapes and a flat surface at different distances from the particle. In order to evaluate the influence of the wall on the drag force at least 6 distances h were modeled.

Spherical, cylindrical, conical, prolate spheroid and hemispherical particles were assayed. These geometries were chosen as the model was made in an axisymmetric domain which limits the types of non-spherical geometries that can be used, and in order to take into account typical fillers in polymeric materials such as short fibers, different carbon structures (carbon black, carbon nanotubes, graphite), and magnetic particles (barium hexaferrite) [11,14].

Isometric perspective views of the particles are shown in Fig. 1. For particles geometries containing flat faces, one of these faces was oriented parallel to the surface wall in order to consider extreme situations.

To compare simulation results for the “non-spherical particles” with those for the sphere, the aspect of the “non-spherical particles” was designed to be equivalent, in one dimension, to the sphere radius R. All the conditions used are summarized in Table 1. In the case of the cylinder, the values were adjusted to obtain an equivalent sphere volume, and in the case of the prolate spheroid particle, the projected area was considered to be equivalent to the sphere projected area.

The sphericity Φ of the particles was calculated as follows [15]:

$$\Phi = \frac{6V_p}{D_{eq}A_p} \tag{1}$$

where V_p is the volume of the particle, A_p is the surface of the particle and D_{eq} is the equivalent diameter of the sphere of the same volume of the particle.

At least fifteen growth velocities (v) in the range of 1×10^{-16} m/s to 10^{-10} m/s were considered, covering the range of velocities where isotactic polypropylene is able to produce impurity segregation in spherulitic crystallization for micrometric particles [16]. Therefore, corresponding Re values were between 1×10^{-21} and 1×10^{-13}.

Table 1
Particles dimensions and surface shape.

Particle shape	Thickness (T) [μm]	R_{ext} [μm]	Surface shape	Sphericity Φ
Circular disk	$R/10$	–	Flat	0,323
Hemisphere	–	–	Flat	0,840
Truncated cone	$R/10$	R + (R/10)	Flat	0,513
Cylinder	$R/0.75$	–	Flat	0,857
Prolate spheroid	200 (c = 100)		Flat	0,930
Sphere	–	–	Flat, concave and convex	1

The boundary conditions in the model were: i) constant fluid velocity in the surface taken as a sink, ii) no-slip condition on the particle surface and iii) other boundaries: free. Newtonian fluid in a laminar flow regime, ($Re \ll 1$).

The particle radii (R) simulated were 50 μm, 10 μm and 1 μm; and the values of $h/2R$ were: 0.0001, 0.01, 0.05, 0.1, 0.5 and 1.

The physical system was simulated on an axisymmetric model which has been previously validated [17]. Similar flow behavior was found and drag force results for three dimensional and axisymmetric models were very close, with a small difference of 0.13%.

The numerical solutions of the problem includes the equations of conservation of mass and momentum. The domain was discretized using 30,000 and 50,000 quadrilateral elements, with second order interpolation functions for the velocity and first order for the pressure. The resulting system of equations was solved employing the Picard method [18]. The fluid flow was assumed to be that for a viscous fluid polymer at zero shear viscosity. Polymers at very slow shear rates display complete Newtonian behavior, and Stokes' law is recovered [10]. In all the cases, the viscosity (μ) of the melt was assumed to be constant and uniform with a value of $1 \times 10^{+3}$ Pa.s (properties of isotactic polypropylene), and a density (δ) of 2700 kg/m^3 and 900 kg/m^3 for particle and melt, respectively [19–20]. The drag force onto the particle was calculated numerically from the velocity field in the fluid flow model by solving the full Navier Stokes equations by a finite element method (Eq. (2)).

$$F_i = \int_S \varphi \overline{\sigma_i} dS = \int_S \varphi \sigma_{ij} n_j dS \tag{2}$$

where, F_i is the component of the force in the i-th direction, n_j is the versor in the j-th direction, σ_{ij} is the stress tensor, φ is the column vector of interpolation functions, and dS is the differential surface. The integration was performed on the whole surface S of the particle.

The stress tensor was obtained from the velocity field using the following equation:

$$t_i = \sigma_{ij} n_j, \qquad \sigma_{ij} = -p\delta_{ij} + \mu(u_{i,j} + u_{j,i}) \tag{3}$$

where p is the pressure term, μ is the viscosity and $u_{i,j}$ and $u_{j,i}$ are the velocity gradients of the i and j components in the j and i directions, respectively.

3. Results and Discussion

The results of the drag force as a function of the separation distance h were rearranged to obtain dimensionless values (Eq. (4)) in order to compare with empirical expressions and for a better visualization.

$$\frac{F_{dSIM}}{6\pi\mu v R} = f\left(\frac{R}{h}\right) \tag{4}$$

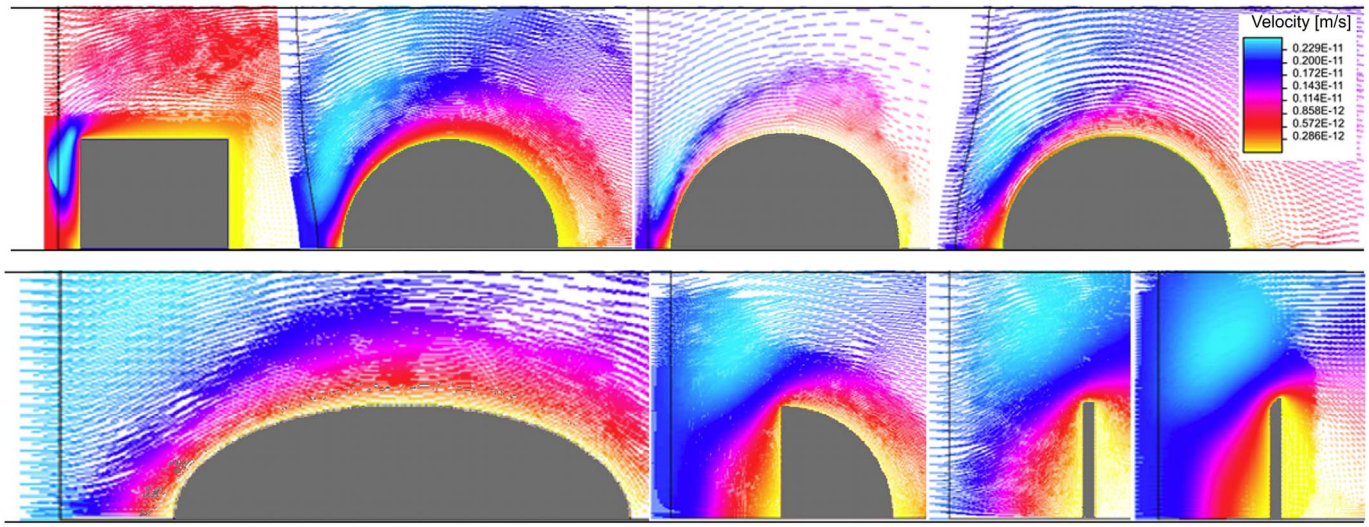

Fig. 2. Fluid flow field at a distance h of 1×10^{-5} m, for cylindrical and spherical particles and at a distance h of 5×10^{-5} m for prolate spheroid, hemispherical, circular disk and truncated cone particles at the growth velocity of 2×10^{-12} m/s.

where F_{dSIM} is the drag force calculated from the simulation, h is the distance from the particle to the wall, v is the velocity of the fluid and R the radius of the particle as it was presented in Table 1.

These results were calculated for each particle geometry and a flat surface. In addition a model with a spherical particle and two different surface shapes; concave and convex was consider. A typical flow field is shown in Fig. 2. The fluid flow was continuous around each particle with no separation lines and very regular with a velocity that increased in the narrow gap between particle and interface. The results obtained at a velocity of 2×10^{-12} m/s are presented as a function of R/h in Fig. 3, as an example.

The experimental results of Ambari et al. for a spherical particle were added in Fig. 3. Our simulation results for spherical particles moving towards a flat surface are in good agreement with Ambari's results confirming the validity of our model.

In general, two different behaviors can be observed in Fig. 3. For values of $R/h < 5$ no significant effect of the configuration was observed. For values higher than $R/h = 5$, each geometry showed a different trend. The drag forces were weaker in the case of spherical particles, especially when the surface was convex. Nevertheless, the behavior showed a similar trend when the value of the particle-interface distance h was higher than R. Hence, the highest values of the drag force were found when the particle-interface distance h was the lowest and the geometry corresponded to a non-spherical particle with a flat face.

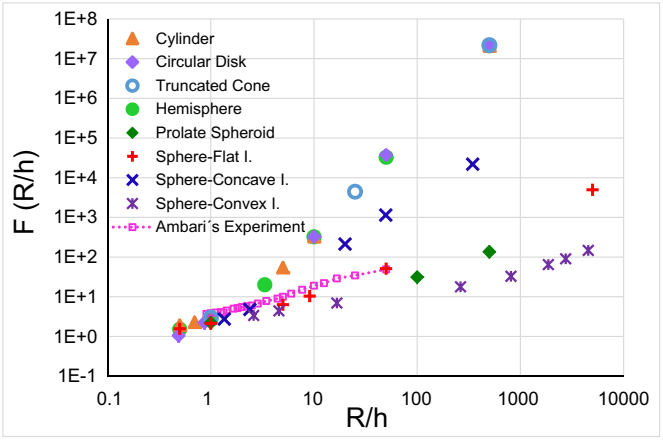

Fig. 3. $F(R/h)$ at a velocity of 2×10^{-12} m/s as a function of R/h.

Therefore, the limit distance h above which the effects of the surface onto the particle started to be negligible at small Reynolds numbers could be established.

In addition, the above results were compared with typical C_d values reported in the literature as it is shown in Fig. 4a. For a better analysis, the results were presented using the relation C_{dth}/C_{di}, where C_{dth} is the typical theoretical value of $24/R$ in Stokes regime and C_{di} corresponds to [3]:

$$C_{di} = \frac{8\, F_{dSim}}{\delta \pi v^2 (2R)^2} \tag{5}$$

It can be observed in Fig. 4a, that at higher values of $h/2R = 1$ (particle far from the wall), C_d values obtained from the simulation were in good agreement to typical reported values. On the other hand, as $h/2R$ decreases (particle approaching to the wall) $C_{dth}/C_{di} < 1$, implying that the drag force increases respect to theoretical values and hence, sedimentation velocity decreases. Therefore, the results obtained here, demonstrate that spherical particles and, particularly, when the surface is convex, sustain lower drag forces and are more prone to sedimentation.

Moreover, simulation results were compared with four analytical expressions: the Stokes equation (F_d) (Eq. (6)) and the Modified Stokes equation for spherical particles (F_{d-SM}) (Eq. (7)), for hemispherical particles (F_{d-SH}) (Eq. (8)) and for circular disks (F_{d-SC}) (Eq. (9)) [4,6–7].

$$F_{d-S} = 6\pi\mu v R \tag{6}$$

$$F_{d-SM} = \frac{6\pi\mu v R^2}{h} \tag{7}$$

$$F_{d-SH} = \frac{3\pi\mu v R^4}{2h^3} \tag{8}$$

$$F_{d-SC} = 16\mu v R \tag{9}$$

The following relations were employed (Fig. 4b); F_{dSim}/F_{d-SM}, F_{dSim}/F_{d-S}, F_{dSim}/F_{d-SH}, F_{dSim}/F_{d-SC} and F_{dSim}/F_{dSim} for a better understanding. The relation $F_{dSim}/F_{dSim} = 1$, which correspond to a perfect correlation.

Fig. 4b shows that some analytical expressions such as Stokes equation lose accuracy with the proximity to the wall but are adequate far from the wall. On the other hand, other expressions such as Modified Stokes equation for spherical particles are more suitable close to

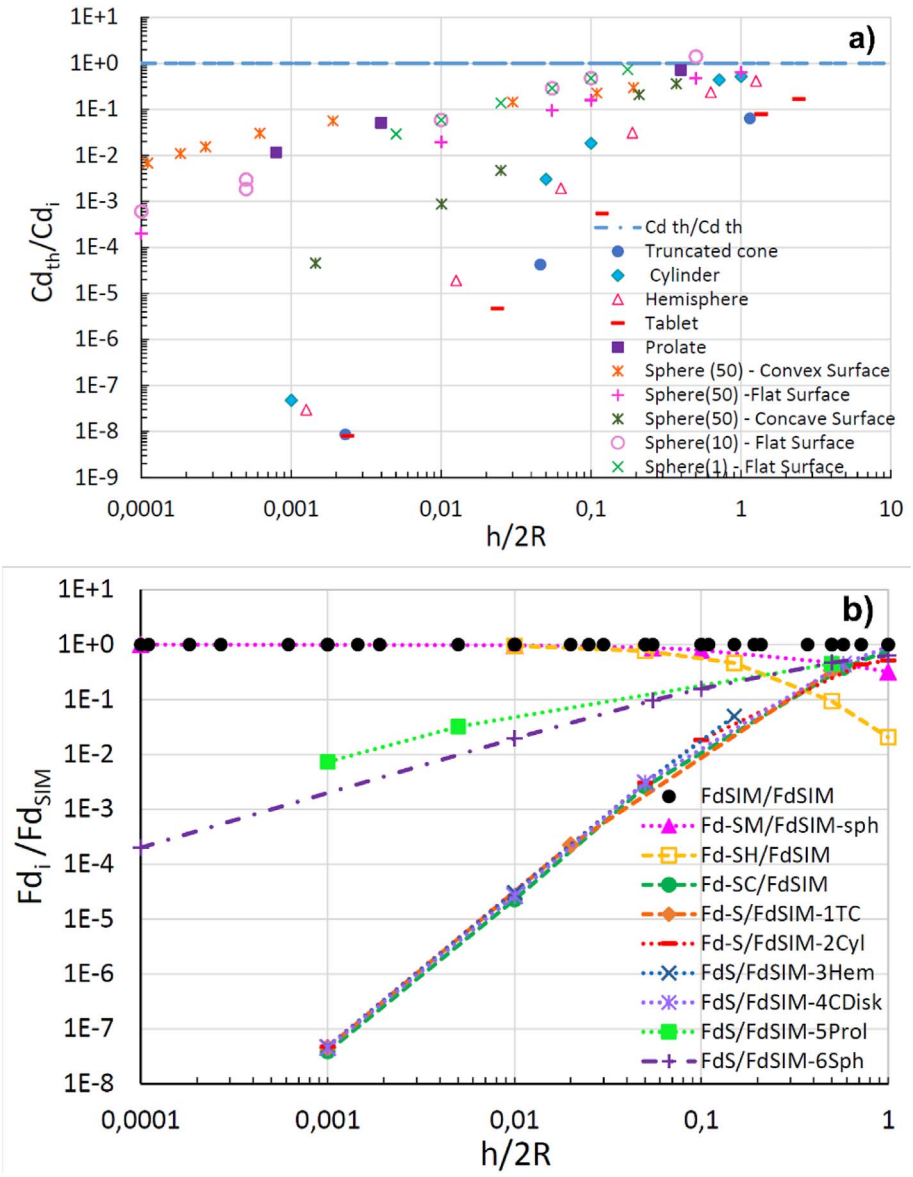

Fig. 4. a) Comparison between theoretical and simulation results of drag coefficients for different particle geometries (C_{dth}/C_{di} as a function of $h/2R$) b) Comparison of the simulation results with four analytical expressions for the drag force for different particle geometries and a plane surface wall.

the wall. Hence, the validity range of the expressions could be established by comparing the numerical results with the four analytical formulations.

As it was discussed above, these results showed two well-defined tendencies. The results from the Stokes Equation (Eq. (6)) for all particles and from analytical expressions for circular disks (Eq. (9)), lost accuracy at values of h smaller than R. On the other hand, accurate approximations were obtained for values of h higher than R. Moreover, the Modified Stokes equation is a good approximation for spherical particles and a flat surface. Simulation and analytical results for hemispherical particles were in good agreement only for values of h smaller than $0.3R$. The results for prolate spheroid particles presented intermediate behavior between spherical particles with flat surface and convex surface, indicating the relevance of the shape of the channel and the distance between the particle and the surface. Drag forces for non-spherical particles near a wall surface were accurately calculated here for the first time using computational modelling.

4. Conclusion

From the results obtained in this work, the following conclusion can be drawn.

Drag forces on a particle moving towards a wall in Stokes regime changes as a function of surface distance. Drag forces are affected by: i) the shape of the particles, ii) distance to the wall and mainly iii) shape of the channel between particle and wall. Hence, spherical particles flowing near a convex wall are the particles most prone to sedimentation among the different particles investigated.

The range of applicability of analytical expressions could be determined.

The model presented here is useful to: i) solve problems of the motion of a body near a solid wall, ii) provide useful improvements into the hydrodynamics of colloidal solids in confinement and other phenomena that need accurate calculations and iii) validate the empirical approaches using analytical approximations.

Acknowledgments

The authors want to thank the National Research Council of Argentina, the University of Buenos Aires (UBACYT 2014–2016, 20020130200282BA) and the FONCyT (PICT 2014-1955) for financial support of this investigation.

References

[1] R. Tuinier, T.H. Fan, T. Taniguchi, Depletion and the dynamics in colloid-polymer mixtures, Curr. Opin. Colloid Interface Sci. 20 (2015) 66–70, http://dx.doi.org/10.1016/j.cocis.2014.11.009.

[2] W. Zhong, A. Yu, X. Liu, Z. Tong, H. Zhang, Dem/cfd-dem modelling of non-spherical particulate systems: theoretical developments and applications, Powder Technol. 302 (2016) 108–152.

[3] E. Loth, Drag of non-spherical solid particles of regular and irregular shape, Powder Technol. 182 (3) (2008) 342–353.

[4] S. Tran-Cong, M. Gay, E.E. Michaelides, Drag coefficients of irregularly shaped particles, Powder Technol. 139 (1) (2004) 21–32.

[5] Y. Chen, J.R. Third, C.R. Müller, A drag force correlation for approximately cubic particles constructed from identical spheres, Chem. Eng. Sci. 123 (2015) 146–154.

[6] A. Hölzer, M. Sommerfeld, New simple correlation formula for the drag coefficient of non-spherical particles, Powder Technol. 184 (3) (2008) 361–365.

[7] G.J. Rubinstein, J.J. Derksen, S. Sundaresan, Lattice Boltzmann simulations of low-Reynolds-number flow past fluidized spheres: effect of Stokes number on drag force, J. Fluid Mech. 788 (2016) 576–601, http://dx.doi.org/10.1017/jfm.2015.679.

[8] W. Stankiewicz, M. Morzynski, K. Kotecki, B.R. Noack, On the need of mode interpolation for data-driven Galerkin models of a transient flow around a sphere, Theor. Comput. Fluid Dyn. (2016) 1–16, http://dx.doi.org/10.1007/s00162-016-0408-7.

[9] A. Ambari, B. Gauthier-Manuel, E. Guyon, Wall effects on a sphere translating at constant velocity, J. Fluid Mech. 149 (1984) 235–253.

[10] J. Happel, H. Brenner, Low Reynolds Number Hydrodynamics, (1983), http://dx.doi.org/10.1016/0009-2509(66)85045-5.

[11] R. Niu, J. Gong, D. Hua Xu, T. Tang, Z. Yan Sun, The effect of particle shape on the structure and rheological properties of carbon-based particle suspensions, Chin. J. Polym. Sci. (2015) 1550–1561, http://dx.doi.org/10.1007/s10118-015-1704-1 (English Ed. 33).

[12] A.V. Catalina, S. Mukherjee, D.M. Stefanescu, A Dynamic Model for the Interaction Between a Solid Particle and an Advancing Solid/Liquid Interface, (October 31, 2000), pp. 2559–2568.

[13] C.E. Schvezov, Dynamic Calculations for Particle Pushing. Solidification 1999, TMS, 1999, pp. 251–261.

[14] C. Materials, Conducting Polymer Hybrids, (2017), http://dx.doi.org/10.1007/978-3-319-46458-9.

[15] S. Sahin, S. Sumnu, Size, shape, volume, and related physical attributes, Physical Properties of Foods (2006) 1–37.

[16] D. Xu, Z. Wang, J.F. Douglas, Crystallization-induced fluid flow in polymer melts undergoing solidification, Macromolecules 40 (2007) 1799–1802, http://dx.doi.org/10.1021/ma0628174.

[17] M. Rosenberger, E. Agaliotis, C. Schvezov, Numerical modeling of the interaction of particles with solidifying interfaces (Solidification Processing of Metal Matrix Composites: Rohatgi Honorary Symposium), (2006), pp. 309–320.

[18] S.C. Chapra, R.P. Canale, Numerical Methods for Engineers, (2012).

[19] R.H. Perry, D.W. Green, Perry's Chemical Engineers' Handbook, McGraw-Hill Professional, 1999.

[20] D.W. Van Krevelen, K. Te Nijenhuis, Properties of Polymers: Their Correlation With Chemical Structure; Their Numerical Estimation and Prediction From Additive Group Contributions, Elsevier, 2009.